JACS
JOURNAL OF THE AMERICAN CHEMICAL SOCIETY
Article
pubs.acs.org/JACS

A Segregated, Partially Oxidized, and Compact Ag_{10} Cluster within an Encapsulating DNA Host

Jeffrey T. Petty,*[,†,§] Orlin O. Sergev,[†] Mainak Ganguly,[†] Ian J. Rankine,[†] Daniel M. Chevrier,[‡,§] and Peng Zhang[‡]

[†]Department of Chemistry, Furman University, Greenville, South Carolina 29613, United States
[‡]Department of Chemistry, Dalhousie University, Halifax, Nova Scotia B3H 4R2, Canada

Supporting Information

ABSTRACT: Silver clusters develop within DNA strands and become optical chromophores with diverse electronic spectra and wide-ranging emission intensities. These studies consider a specific cluster that absorbs at 400 nm, has low emission, and exclusively develops with single-stranded oligonucleotides. It is also a chameleon-like chromophore that can be transformed into different highly emissive fluorophores. We describe four characteristics of this species and conclude that it is highly oxidized yet also metallic. One, the cluster size was determined via electrospray ionization mass spectrometry. A common silver mass is measured with different oligonucleotides and thereby supports a Ag_{10} cluster. Two, the cluster charge was determined by mass spectrometry and Ag L_3-edge X-ray absorption near-edge structure spectroscopy. Respectively, the conjugate mass and the integrated white-line intensity support a partially oxidized cluster with a +6 and +6.5 charge, respectively. Three, the cluster chirality was gauged by circular dichroism spectroscopy. This chirality changes with the length and sequence of its DNA hosts, and these studies identified a dispersed binding site with ∼20 nucleobases. Four, the structure of this complex was investigated via Ag K-edge extended X-ray absorption fine structure spectroscopy. A multishell fitting analysis identified three unique scattering environments with corresponding bond lengths, coordination numbers, and Debye−Waller factors for each. Collectively, these findings support the following conclusion: a Ag_{10}^{+6} cluster develops within a 20-nucleobase DNA binding site, and this complex segregates into a compact, metal-like silver core that weakly links to an encapsulating silver−DNA shell. We consider different models that account for silver−silver coordination within the core.

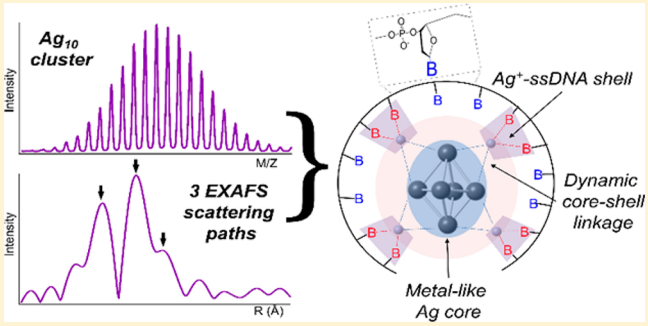

INTRODUCTION

Silver clusters with diameters ∼1 nm are chromophores with molecule-like, nonplasmonic spectra.[1−7] They absorb across the optical spectrum and can strongly emit, so they are distinct from bulk silver and silver nanoparticles.[8] Their spectra depend on the number of silver atoms, so the synthesis of atomically precise clusters opens the possibility of a suite of programmable chromophores that is distinct from other fluorescent labels.[9−14] Specific species are formed via adsorbates that coordinate the cluster surface and thus inhibit agglomeration. These ligands control both the cluster size and electronic spectra, as illustrated by thiols that strongly coordinate silver clusters and shift their optical spectra.[15] Our studies focus on DNA ligands that develop silver clusters in aqueous solution.[16−22] These polymeric ligands coordinate Ag^+ via their nucleobases, and they facilitate silver agglomeration when the locally concentrated Ag^+ adducts are chemically reduced.[23−26] The encapsulated clusters develop discrete and sparsely organized electronic states and become optical chromophores with several distinguishing characteristics. They have high molecular brightness due to extinction coefficients of $\sim 10^5$ M^{-1} cm^{-1} and fluorescence quantum yields as high as 90%, strong and robust emission due fluorescence lifetimes ∼1 ns and weakly coupled excited electronic states, and emission that can be optically modulated via transiently populated dark states.[27−30] Finally, their spectra span the visible and near-infrared spectral regions and are encoded by the primary sequence and secondary structure of the DNA host.[28,29,31−33]

Our studies focus on a specific cluster with $\lambda_{max} \approx 400$ nm and with low emission, which exclusively develops within single-stranded oligonucleotides. We are interested in this species because it is a chameleon-like precursor that can be transformed into different fluorescent clusters via DNA hybridization. The single-stranded DNA host hybridizes with a complementary strand, and the violet precursor switches to a fluorescent cluster with $\gtrsim$ 100-fold stronger emission.[25,34] The fluorescence spectrum is encoded by the DNA sequence. Furthermore, the violet precursor is regenerated when the duplex denatures.[35]

Such dim/bright cluster pairs are the foundation of a new class of optical sensors, and our goal is to address the

Received: December 15, 2015
Published: February 28, 2016

ACS Publications © 2016 American Chemical Society

DOI: 10.1021/jacs.5b13124
J. Am. Chem. Soc. 2016, 138, 3469−3477

underlying changes in electronic structure.[7,19,20,32] The present studies focus on the violet cluster complexed with a 20-nucleotide DNA strand, and we used three techniques to characterize the cluster stoichiometry, oxidation state, ligand environment, and structure. One, electrospray ionization mass spectrometry measured the silver stoichiometry with the 20-nucleotide and a longer DNA strand, and a common, dominant empirical stoichiometry supports a specific cluster size. Mass spectrometry also quantitated the number of H^+ bound to the phosphate backbone, and a loss of H^+ signifies a partially cationic cluster. Two, X-ray absorption spectroscopy studies revealed the cluster oxidation state and fundamental bonding interactions in the cluster/DNA complexes in the native aqueous environment.[36] The Ag L_3-edge X-ray absorption near-edge spectra gauged the cluster charge via the occupancy of the valence electronic states of silver. The extended X-ray absorption fine-structure region of the Ag K-edge spectra revealed three scattering paths, and these were ascribed to silver-nucleobase and two types of silver−silver interactions. Three, circular dichroism spectroscopy probed the ligand environment because the chiroptical response of the cluster changes with the length and sequence of the DNA host. These studies support an extended DNA binding site. Collectively, our studies suggest that the violet cluster/DNA complex segregates into distinct components: an encapsulating DNA−silver shell, a metal-like silver core, and a dynamic core−shell linkage. We discuss specific structural models based on these interactions.[37−39]

EXPERIMENTAL SECTION

We followed the experimental protocol from our earlier studies, and the key aspects are summarized.[25,40,41] The 20-nucleotide DNA strand used for most of these studies was CCCCAACTCCTTCCCGCCAC, where the strand polarity is 5′ → 3′. The clusters were prepared using $AgNO_3$ (Acros), and the reducing agent was $NaBH_4$ (Aldrich). These reagents were used as received. Violet cluster conjugates were formed by combining 8 equiv of Ag^+ with 30 μM oligonucleotide in water. This solution was combined with BH_4^-, and the violet cluster was favored by exposing the solution to 500 psi O_2 at room temperature for 3 h. For mass spectrometry studies, these solutions were dialyzed to achieve 10^2−10^4 dilution of lower molecular weight species. Mass spectra were collected using Q-TOF G2-S (Waters) and analyzed with MassLynx V4.1. Samples were diluted with water to 0.3 μM oligonucleotide concentration and were infused via a syringe pump operated at 20 μL/min. The spectra were acquired in the negative ion mode with a capillary voltage of −2.7 kV, sampling cone voltage of −15 V, extraction cone voltage of 10 V, a cone gas flow of 45 L/h of cone gas, and a desolvation gas flow of 450 L/h. The source temperature was 80 °C, and the desolvation temperature was 130 °C. Mass calibration was performed using aggregates of sodium formate in the $400 < m/z < 2000$ range. Each mass spectrum was an average of 290 scans collected in V mode, and these spectra were processed with the MassLynx software. The peaks associated with the different charge state peaks were converged to the zero charge state to reconstitute a mass spectrum of the neutral species.[42−44] Ag K-edge (25514 eV) and Ag L_3-edge (3351 eV) X-ray spectra were collected of the Ag-DNA conjugates in buffered aqueous solution at the with a cluster concentration of ∼5 mM. The PNC-XSD beamline (Sector 20-BM) at the Advanced Photon Source, Argonne National Laboratory (IL, USA), was used to collect Ag K-edge EXAFS data. Experiments were conducted at room temperature under ambient conditions. Data were collected for the solution-phase sample in fluorescence mode using a 12-element fluorescence detector. Multiple scans were averaged to achieve minimal experimental noise in the late k region of the EXAFS data. Ag L_3-edge XANES were collected at the SXRMB end station at the Canadian Light Source (Saskatoon, SK, Canada). Experiments were conducted in solution-phase at room temperature under a stream of N_2 gas. Data were collected in fluorescence mode with multiple scans acquired to ensure reproducibility and to minimize experimental noise in the XANES region. All XAS data were background subtracted, normalized, and transformed to k- and R-space using standard data reduction protocols (Figure S13).[45] Simulated scattering paths used to fit the Ag K-edge EXAFS data were generated using FEFF8.2 computational software.[46] Reported uncertainties for EXAFS fitting results were computed from off-diagonal elements of the correlation matrix, which were weighted by the square root of the reduced chi-squared value obtained for each simulated fit. The amount of experimental noise was also taken into consideration for each Fourier transformed R-space spectrum from 15−25 Å.[47] Linear combination fitting of Ag L_3-edge XANES data was conducted using Athena and Ifeffit software.[48,49] The linear combination fit was conducted from −20 to 30 eV with respect to the absorption edge (E_0 for Ag L_3), and an R-factor statistic of 0.017 was determined from the fitting result to indicate the goodness of fit.[50]

Absorption spectra were acquired with a Cary 50 (Varian) at a scan rate of 600 nm/min using an appropriate buffer baseline and using plastic cuvettes (BrandTech). Circular dichroism spectra were acquired with a DSM 17 CD spectrophotometer (Olis). The spectra were collected from 600−220 nm using quartz cells with a path length of 1 cm using a scanning rate of ∼150 nm/min. A background spectrum of water was collected and subtracted from three averaged scans of the sample. Size exclusion chromatograms were collected with a Prominence high performance liquid chromatography system (Shimadzu) using a 300 × 7.8 mm^2 BioSep-SEC-S2000 column (Phenomenex), having 5 μm particles and a pore size of 145 Å. The mobile phase was buffered at pH = 6.5 with 10 mM citrate/citric acid that was supplemented with 300 mM $NaClO_4$ to minimize solute interactions with the stationary phase.[51,52]

RESULTS

Cluster Stoichiometry. Our previous studies established the cluster size and undergird our new investigations, so we first summarize these results.[25] The violet cluster develops in a 20-nucleotide DNA strand with concentrations $\lesssim$ 10 Ag^+:DNA and high oxygen pressures. We chose these conditions because they eliminate competing species and favored the violet cluster (Figure S1). The crude reaction mixture was characterized by electrospray ionization mass spectrometry, and two types of DNA strands were identified (Figure 1A, inset). The molecule with a mass of 5878 amu is the native DNA, while the heavier species with a mass of 6951 amu is the same strand with 10 silvers. Three observations linked this gaseous DNA−silver complex with the aqueous DNA−violet cluster conjugate. First, the reaction mixture was also analyzed by size exclusion chromatography, and this technique correspondingly identified two types of DNA strands in aqueous solution (Figure S2). The bound and free strands were distinguished by their electronic spectra, and their relative amounts were 2.5:1, respectively, which compares favorably with the ratio of 3.3:1 for the gaseous strands (Figure 1A, inset). This similarity suggests that the distribution of species in aqueous solution was faithfully mapped in the gas phase. Second, the absorbance of the DNA-violet cluster complex increased from 2 to 8 Ag^+:DNA, and the abundances of the gaseous 10-Ag/DNA complex proportionally increased.[25] This correlation between the aqueous and gaseous amounts of the complexes further connects these two species. Third, the gaseous complex survived a range of collision energies, temperatures, and gas flow rates.[53] This stability suggests that the cluster/DNA conjugate retained its integrity not only in the gas phase, but also from its original aqueous state. This 10-Ag stoichiometry is

DOI: 10.1021/jacs.5b13124
J. Am. Chem. Soc. 2016, 138, 3469−3477

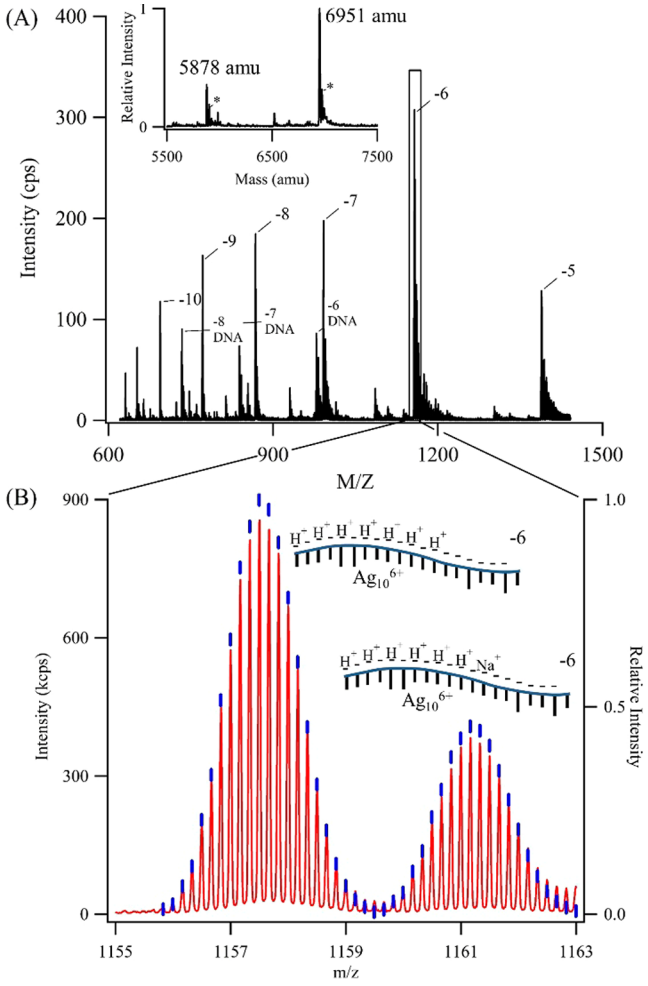

Figure 1. (A) Mass:charge spectrum of a violet cluster−DNA sample. The peaks labeled −11 to −5 correspond to the respective ions of the Ag10/DNA complex. The peaks labeled −10 DNA to −5 DNA correspond to the respective ions of the native DNA strand. The inset shows the composite, zero-charge spectrum that identifies the native DNA at 5878 amu and the DNA with 10 Ag at 6951 amu. The *peaks represent Na^+ adducts. (B) Expanded view of the −6 charge state. The leftmost set of peaks corresponds to the complex with only H^+ bound to the phosphates. The blue tick marks represent the predicted masses based on the molecular formula of the oligonucleotide with 10 silvers and 6 fewer hydrogens. The rightmost set of peaks corresponds to the same ion with 1 Na+ that replaces 1 H^+. The precisions between the observed and predicted masses of the isotopologues are 0.3 ± 0.4 and 0.4 ± 0.4 ppm, respectively.

supported by in situ elemental analysis and calorimetry studies.[25]

The mass spectra measured the empirical silver:DNA stoichiometry, and an alternate DNA host supported the same relative stoichiometry. The original 20-nucleobase strand was appended with eight additional or 40% more nucleobases, and these added nucleobases increased the number of potential coordination sites for the cluster (Figure S3A).[54,55] Despite its longer length, the longer strand mimicked its parent in two respects. One, the dominant species in both mass spectra were the respective oligonucleotides with 10 additional silvers. Two, both complexes exhibited similar absorption and circular dichroism spectra (Figures 3 and S3, Strands 1 and 3). These observations suggest that the 10 silvers agglomerated and formed a single cluster within a common DNA binding site. Collectively, these experiments indicate that the violet chromophore is the cluster Ag_{10}.

Cluster Charge. The violet cluster preferentially forms with the oxidizing agents O_2 and H_2O_2.[25] This reactivity suggests that the cluster is cationic, and the charge was determined via mass spectrometry and X-ray absorption spectroscopy measurements. Mass spectrometry shows that the mass of the oligonucleotide−cluster complex (6951 amu) was 6 amu lower than the combined mass of the native oligonucleotide (5878 amu) and 10 silvers (1079 amu) (Figure 1). We attribute this deficit to missing protons and ultimately to the cluster charge.[30,56,57] During desolvation, different numbers of H^+ bound to the phosphate backbone and yielded a range of ions with net charges of −5 to −11 (Figure 1A).[44] The number of H^+ was deduced from fine structure in the mass spectrum (Figure 1B). A given ion has a range of isotopologues due to its natural distribution of isotopes, and the pattern of peaks is dictated by the numbers and types of atoms, that is, the molecular formula.[30,57−60] Our analysis is based on the neutral oligonucleotide with the formula $C_{187}H_{244}O_{116}N_{65}P_{19}$, and we focus on its two isoelectronic ions with −6 charges. The unlabeled oligonucleotide has a peak pattern that was reproduced by the formula $C_{187}H_{238}O_{116}N_{65}P_{19}^{-6}$ (Figure S5). Thus, this ion developed its −6 charge because it lost 6 H^+ relative to the fully protonated strand. The corresponding Ag_{10}-labeled oligonucleotide had a denser peak pattern due to its ten additional silvers with natural abundances of 51.8% ^{107}Ag and 42.8% ^{109}Ag (Figure 1B). The positions and intensities of these peaks were reproduced with the formula $C_{187}H_{232}O_{116}N_{65}P_{19}Ag_{10}^{-6}$. Thus, this ion lost six more H^+ in relation to its unlabeled counterpart, and these missing protons account for the mass deficit in the composite mass spectrum (Figure 1A, inset). Alternate formulas with ±1 H^+ predicted markedly different distributions with larger standard deviations and thus substantiate the loss of specifically 6 H^+ (Figure S6).[61] We propose that the cluster has a + 6 charge, so the oligonucleotide host maintained its overall −6 charge by shedding 6 additional H^+. The other seven ions with net charges of −5 and −7 to −11 also lacked 6 H^+ relative to their unligated counterparts, so these consistent offsets support a constant +6 oxidation state for the cluster (Figure S7).

Three experiments manipulated the overall DNA charge and indirectly probed the charge of the cluster adduct. First, ammonium acetate shifted the degree of protonation (Figure S8).[62] This salt formed a buffered solution and created less negatively charged ions. The isotopologue distributions again establish that these −4 to −10 charged ions lacked 6 H^+ relative to their unligated counterparts (Figure S9). Two, Na^+ formed complexes that also neutralized the overall DNA charge (Figures 1B and S10). Like H^+, Na^+ is ubiquitous, and it preferentially binds with the phosphate backbone and carries a +1 charge.[63,64] The resulting distributions consistently yielded molecular formulas with the added Na^+ but with 5 instead of 6 fewer H^+. Thus, the net charge offset was again +6, and this charge difference further supports the +6 oxidation state for the cluster. Three, the longer 28-nucleotide strand also formed the violet Ag_{10} cluster (Figure S3A). This strand has 40% more phosphates but still produced the silver cluster complexes with 6 fewer H^+ than the unligated counterpart (Figure S3B,C). Collectively, the analysis of these different charge states and different complexes supports a gaseous Ag_{10} cluster with 6 oxidized Ag^+ and 4 reduced Ag.

DOI: 10.1021/jacs.5b13124
J. Am. Chem. Soc. 2016, 138, 3469−3477

We also measured the cluster oxidation state using Ag L_3-edge X-ray absorption near-edge structure (XANES) spectra.[36] These investigations complemented the mass spectrometry studies because they characterized the cluster/DNA complex in its native aqueous environment (Figure 2). The white-line

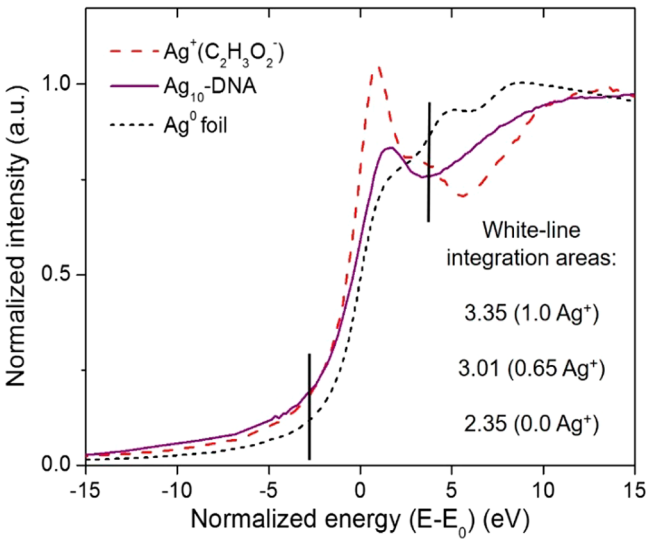

Figure 2. Ag L3-edge XANES of the Ag10-DNA conjugates in aqueous solution (solid purple line). The white-line integration analysis (between −3 and 3 eV, indicated with black lines) used two references: ionic silver acetate (long dashed red line) and silver metal (short dashed black line).

feature reflects the dipole-allowed promotion of $2p_{3/2}$ core electrons to partially occupied 5*s*/4d valence states. The intensity of this transition inversely varies with the occupancy of the valence states and was analyzed in relation to bulk silver metal (Ag^0) and the ionic salt silver acetate (Ag^+) references.[36] The area under the white-line transition was integrated from ±3 eV of the absorption edge and compared with the two reference materials. Linearly interpolating the integrated area from the spectrum of the cluster gave ∼35% Ag^0 and ∼65% Ag^+. This proportion supports a 6+ overall charge for Ag_{10} cluster, so the charge analysis from XANES and mass spectrometry measurements favorably agree. This partially oxidized cluster signifies two types of silver within the complex, and we subsequently considered their organization.

Ligand Environment. The DNA strand is the scaffold for the violet cluster, and we addressed its capacity for silver from two perspectives. First, mass spectra enumerated the number of DNA-bound Ag^+ (Figure S11). We studied Ag^+−DNA complexes because the cluster is largely oxidized. Furthermore, Ag^+ binds the exposed nucleobases like silver clusters.[54,55] The affinity constant is $\sim 10^6$ M^{-1}, so the oligonucleotide forms stable complexes with Ag^+ because our experiments used $\sim 10^2$ μM Ag^+ and $\sim 10^1$ μM DNA concentrations.[24,25] Our studies identified specific complexes that developed from opposing directions. First, Ag^+ and DNA were combined with an initial concentration of 12 Ag^+:DNA and then diluted with 100 and 10 000 volumes of water (Figure S11A). Weakly bound complexes dissociated with dilution, and only species with relatively smaller stoichiometries of 4−7 Ag^+:DNA survived. The dominant species had 5−6 Ag^+:DNA, but their abundances did not follow a Poisson distribution. This disparity between the observed and random Ag^+ distributions further substantiated the chemical stability of these complexes. As an aside, we note that the isotopologue distributions for these complexes showed that the DNA-bound Ag^+ displaced an equivalent number of H^+ from the phosphate backbone (Figure S11C). This charge balance supports the earlier mass spectral analysis of the cluster oxidation state (Figure 1). Second, Ag^+ and DNA were combined with a lower concentration of 3 Ag^+:DNA and then diluted (Figure S11B). Complexes with relatively higher concentrations of 4−6 Ag^+:DNA emerged with these stoichiometries. Thus, opposing initial concentrations converged to complexes with 4−7 Ag^+:DNA. This number of Ag^+ is comparable to the number of Ag^+ in the violet cluster.

Second, we also used the chiroptical response of the violet cluster and characterized the cluster binding site (Figure 3).[16,54,55,65] The anisotropy or Kuhn dissymmetry factor κ

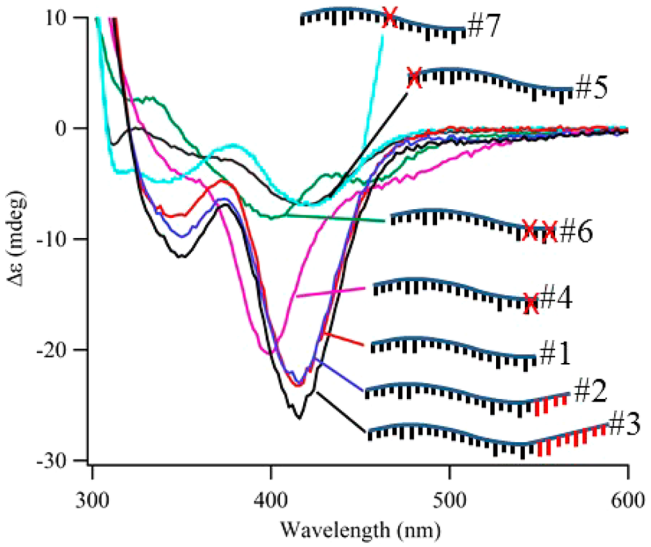

Figure 3. Circular dichroism spectra of violet clusters with the DNA templates from Table 1. In relation to Strand 1, the red X's refer to the deletions and the red appendages refer to additional 3′ nucleobases. The numbers refer to the strand numbers in column 1 of Table 1.

eliminates the concentration dependency in the circular dichroism spectra because it normalizes the differential absorbance (ΔA) using the absorbance (A): $\kappa = \Delta A/A = \theta/(32980 \times A)$, where θ is the ellipticity (mdeg).[54,55,65−68] Our studies measured the anisotropy factors with different DNA strands, and the 20-nucleobase strand provided our reference (Strand 1, Table 1 and Figures 3 and S4). This oligonucleotide produced a violet cluster with $\kappa = 1.2 \times 10^{-3}$, which was comparable to values for other silver clusters encapsulated by DNA and for gold clusters coordinated by chiral thiol ligands.[65,68] Furthermore, the circular dichroism was robust up to 70 °C, and this thermal stability supports a strong cluster−DNA association (Figure S12). Longer and shorter oligonucleotides probed this interaction (Table 1 and Figures 3 and S4). Strands 2 and 3 appended four and eight additional nucleotides onto the 3′ terminus of the parent Strand 1, respectively, and all three strands produced clusters with similar spectra and anisotropies. Thus, added nucleobases were innocuous and presumably did not interact with the violet cluster. This conclusion is supported by the mass spectrometry studies with Strand 3 (Figure S4). Shorter strands still produced violet clusters with strong absorption but with diminished chirality. Strand 4 removed $A_{19}C_{20}$ from the 3′

DOI: 10.1021/jacs.5b13124
J. Am. Chem. Soc. 2016, 138, 3469−3477

Table 1. Circular Dichroism Anisotropies (κ) with Different DNA Strands[a,b]

strand number	length	sequence	modification	κ ($\times 10^{-3}$)
1	20	5′ $C_1C_2C_3C_4A_5A_6C_7T_8C_9C_{10}T_{11}T_{12}C_{13}C_{14}C_{15}G_{16}C_{17}C_{18}A_{19}C_{20}$ 3′	parent strand	1.2
2	24	$C_1C_2C_3C_4A_5A_6C_7T_8C_9C_{10}T_{11}T_{12}C_{13}C_{14}C_{15}G_{16}C_{17}C_{18}A_{19}C_{20}G_{21}A_{22}T_{23}C_{24}$	add 3′ $G_{21}A_{22}T_{23}C_{24}$	1.4
3	28	$C_1C_2C_3C_4A_5A_6C_7T_8C_9C_{10}T_{11}T_{12}C_{13}C_{14}C_{15}G_{16}C_{17}C_{18}A_{19}C_{20}G_{21}A_{22}T_{23}C_{24}G_{25}A_{26}T_{27}C_{28}$	add 3′ $G_{21}A_{22}T_{23}C_{24}G_{25}A_{26}T_{27}C_{28}$	1.4
4	18	$C_1C_2C_3C_4A_5A_6C_7T_8C_9C_{10}T_{11}T_{12}C_{13}C_{14}C_{15}G_{16}C_{17}C_{18}$	eliminate 3′ $A_{19}C_{20}$	1.0
5	18	$C_3C_4A_5A_6C_7T_8C_9C_{10}T_{11}T_{12}C_{13}C_{14}C_{15}G_{16}C_{17}C_{18}A_{19}C_{20}$	eliminate 5′ C_1C_2	0.6
6	16	$C_1C_2C_3C_4A_5A_6C_7T_8C_9C_{10}T_{11}T_{12}C_{13}C_{14}C_{15}G_{16}$	eliminate 3′ $C_{17}C_{18}A_{19}C_{20}$	0.3
7	18	$C_1C_2C_3C_4A_5A_6C_7T_8C_9C_{10}$---------$C_{13}C_{14}C_{15}G_{16}C_{17}C_{18}A_{19}C_{20}$	eliminate internal $T_{11}T_{12}$	0.4

[a]Refer to Figure 3 for the corresponding circular dichroism spectra. [b]Column 1 is the strand number, column 2 is the length of the oligonucleotide, column 3 is the sequence of the strand, column 4 describes the modification, and column 5 is the measured anisotropy.

terminus and formed a cluster adduct with a shifted circular dichroism and a suppressed κ. Correspondingly, Strand 5 eliminated the 2 $C1C_2$ nucleobases from the opposing 5′ terminus, and this construct yielded more dramatic changes: the absorption red-shifted and diminished, the circular dichroism was significantly quenched, and the anisotropy dropped two-fold. Strand 6 removed the four nucleobases $C_{17}C_{18}A_{19}C_{20}$ and produced a violet cluster with a shifted but still robust absorption but a weak circular dichroism. Strand 7 eliminated $T_{11}T_{12}$, and this internal change also significantly altered the cluster environment. Collectively, these studies identify a break in the cluster binding site at ~20 nucleobases. We suggest that shorter strands have an inadequate number of nucleobases to stabilize the cluster adduct.

Complex Structure and Organization. The Ag K-edge extended X-ray absorption fine structure (EXAFS) spectra examined the structure of the complex from the perspective of the violet cluster adduct. These spectra identified three single scattering paths in a multishell fitting analysis (Figures 4 and S13). Theoretical modeling determined the associated bond distances, coordination numbers, and Debye–Waller factors for each scattering path (Table 2). The first peak (Ag–Nucleobase in Table 2 and Figure 4) is ascribed to a silver–DNA interaction, and its associated bond length suggests that these silvers coordinate with heterocyclic nitrogens in the nucleobases. The 2.24 ± 0.01 Å bond distance matches the length of silver–nitrogen bonds in Ag^+–nucleobase, Ag^+–amine, and Ag–pyridine complexes.[69−73] Furthermore, Ag^+ preferentially complexes the nitrogens versus the oxygens within the nucleobases.[71,74,75] The second peak (Ag–Ag_1 in Table 2 and Figure 4) is ascribed to metal-like bonding between silvers because the 2.743 ± 0.008 Å bond distance is comparable to the 2.889 Å bond distance in cubic closest packed crystals of metallic silver and the 2.82 Å bond distance in the metal core of Ag_{44} nanoclusters.[76−78] This correspondence suggests that these silvers agglomerate and form a recessed core within an encapsulating DNA shell. The third peak (Ag–Ag_2 in Table 2 and Figure 4) is ascribed to long-range silver–silver interactions since the average bond distance of 3.37 Å is comparable to the combined van der Waals radii of 3.44 Å for two silver atoms.[79] This peak suggests that two types silvers are spatially segregated. We suggest that these two silver environments are also distinguished by their oxidation states because the reduced silver partitions into the core while the oxidized silver coordinates with the encapsulating DNA shell.

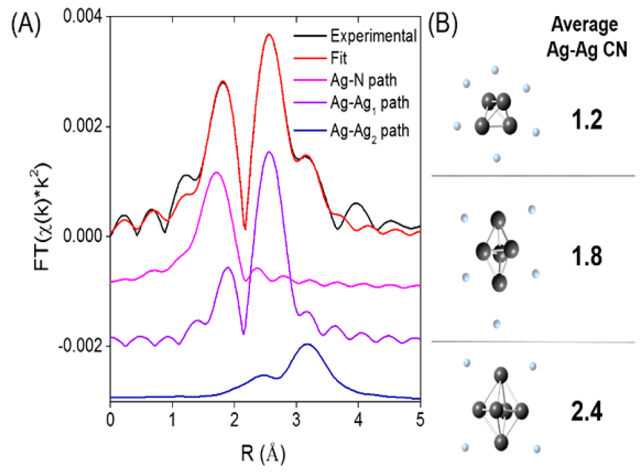

Figure 4. (A) Ag K-edge EXAFS of Ag–DNA conjugates fitted with three individual scattering paths shown separately and (B) proposed Ag core structures and corresponding theoretical CN values (gray atoms and faded blue atoms represent Ag^0 and Ag^+, respectively).

Table 2. Ag K-edge EXAFS Fitting Results for Violet Cluster–DNA Conjugate[a]

scattering shell	CN	R (Å)	σ (Å^2)	ΔE_0 (eV)
Ag–nucleobase	1.02(16)	2.24(1)	0.004(2)	−6(1)
Ag–Ag_1	2.2(3)	2.743(8)	0.011(1)	−6(1)
Ag–Ag_2	3.6(1.7)	3.37(2)	0.026(7)	−6(1)

[a]CN is the coordination number, R is the bond distance, σ is the Debye–Waller factor, and ΔE_0 is the shift in absorption edge energy.

Coordination numbers enumerated each scattering path and thereby helped discern feasible structures (Table 2). The first peak is attributed to a silver–nucleobase bond, and the average of coordination number of 1.02 ± 0.16 silvers:nucleobase is evaluated using two models. First, each of the 10 silvers coordinates one nucleobase:

$$10\ Ag \times \frac{1\ Ag - Nucleobase\ bond}{Ag} / 10\ Ag\ total = 1.0$$

Alternatively, a subset of 5–6 oxidized Ag^+ could preferentially complex the oligonucleotide, as suggested by the mass spectrometry studies of the Ag^+–DNA complexes (Figure S11). Because X-ray diffraction studies indicate that a Ag^+ coordinates two nucleobases, the average coordination number would be 1.0–1.2.[69,80] Both models give reasonable agreement with the observed coordination number, and they share a common feature: the number of coordinated nucleobases is lower than the total number of ~20 nucleobases in the minimal DNA strand (Figure 3). This difference suggests that the polymeric strand intermittently contacts the cluster with intervening unbound nucleobases.

DOI: 10.1021/jacs.5b13124
J. Am. Chem. Soc. 2016, 138, 3469–3477

The second peak is due to silver−silver bonds and has a coordination number of 2.2 ± 0.3. We now consider three scenarios that ultimately support a compact core with interconnected silver−silver bonds. We first evaluate a fully reduced core with 4 Ag^0. A tetrahedral arrangement positions each silver with three neighbors, so the average coordination number is

$$4\ Ag \times \frac{3\ Ag - Ag\ bonds}{Ag} / 10\ Ag\ total = 1.2$$

This predicted value is lower than our experimental value of 2.2, so we progress to 5 Ag with a trigonal bipyramidal geometry. The axial and equatorial silvers bond with 3 and 4 silvers, respectively, so the predicted coordination number is

$$\frac{\left[3\ Ag \times \frac{4\ Ag - Ag\ bonds}{Ag}\right] + \left[2\ Ag \times \frac{3\ Ag - Ag\ bonds}{Ag}\right]}{10\ Ag\ total} = 1.8$$

This coordination number is also lower than the measured value, so we next consider a Ag_6 core. An octahedral geometry arranges these silvers with four nearest neighbors, so the average coordination number is

$$6\ Ag \times \frac{4\ Ag - Ag\ bonds}{Ag} / 10\ Ag\ total = 2.4$$

The latter case gives the best agreement with the observed coordination number, but a fully reduced Ag_6 is outside the distribution of 4 Ag^0 and 6 Ag^+ determined by the mass and XANES spectra. We subsequently consider models with a partially oxidized core that address this discrepancy.

The third peak in the EXAFS spectrum is ascribed to long-range interactions between silvers. Its large coordination number and Debye−Waller factor support multiple and dynamic interactions between distant silvers within the core- and shell-based silvers.

DISCUSSION

Our studies characterized a complex between a specific silver cluster with violet absorption and its 20-nucleobase DNA host. We focused on this particular cluster because it has low emission but can be transformed to different fluorescent silver clusters with ∼100-fold stronger emission. Thus, violet cluster/single-stranded DNA conjugates anchors a new type of optical DNA sensor.[20,32,35,81] We characterized the molecular stoichiometry, oxidation state, ligand environment, and structure of this cluster, and this information will help address its underlying electronic structure. Mass spectra show that a single agglomerated Ag_{10} cluster develops with different DNA strands (Figure 1). Mass and Ag L_3-edge XANES spectra determined comparable oxidation states of +6 and +6.5 for the gas-phase and aqueous complexes, respectively (Figures 1 and 2). Circular dichroism spectra show that the minimum cluster binding site is ∼20 nucleobases (Figure 3 and Table 1). The EXAFS spectra exhibit three single scattering paths, and the associated bond lengths, coordination numbers, and Debye−Waller factors support Ag−nucleobase, metal-like Ag−Ag, and long-range Ag−Ag bonds (Figure 4 and Table 2). These three interactions segregate the cluster, and we now suggest possible structures for the Ag_{10}^{6+} cluster with its 20-nucleobase DNA host.

Metal-like Core. The EXAFS spectrum supports a metal-like core because the 2.743 Å Ag−Ag bond length is similar to the 2.889 Å bond distance in metallic silver (Ag−Ag_1 in Table 2).[76] However, the shorter bond length for the cluster can also signify a partially oxidized core.[76,82] Subvalent silver complexes were once considered to be rare because the individual silvers have fractional oxidation states that conflict with basic bonding theories.[83,84] However, a wide range of these compounds has been synthesized with diverse ligands such as halides, oxides, thiols, peptides, and oligonucleotides.[56,85−90] The first reported example, Ag_2F, and related compounds mimic bulk silver because they have high electrical conductivities at temperatures as low as 20 K.[91−93] Such metallic characteristics may develop because low-lying 5*s*/5p states lie near the Fermi level and can accommodate excess electrons.[92,94] These complexes have relatively short silver−silver bond distances of 2.75−2.85 Å, as does the violet cluster.[82] A partially oxidized core within the violet cluster is also supported by the average Ag−Ag coordination number and the overall cluster charge (Table 2). The observed coordination number of 2.2 is best modeled as a Ag_6 cluster with an octahedral geometry. However, this core is not fully reduced but would need to carry a +2 charge along with 4 peripheral Ag^+. Thus, a $(Ag_6^{2+})-(Ag^+)_4$ arrangement maintains the overall +6 oxidation state of the cluster. However, the four valence electrons in Ag_6^{2+} do not correspond to a stable electron organization based on jellium models, and a similar situation occurs with Au_7^{3+}.[95−98] This molecular cluster partitions into linked tetrahedra with a shared apex, and each subunit has an electron configuration with two valence electrons. Analogously, we suggest that the Ag_6^{2+} cluster may be decomposed into two Ag_3^+ subunits with two electrons each. We suggest that this electronic organization stabilizes the metal-like core.[99] Another example of a subvalent cluster is Ag_6^{4+} with an octahedral geometry, and such species are distinct from the fully reduced cores with other silver cluster−ligand complexes.[77,78]

Irrespective of the detailed structure, the core of the violet cluster has a silver coordination number that signifies interconnected silver bonding and a compact structure. Such a shape is distinct from the elongated structures of other silver clusters.[30,57] These structures were derived from electronic spectra and particle-in-a-box models. This analysis organizes the valence electrons within cylindrical orbitals around a cationic, rod-like core. The longitudinal excitation energies diminish with the length of the molecular rod and increasing silver stoichiometries.[100,101] Molecular dynamic simulations suggest that these atomically sized rods are anchored by the linear array of nucleobases in the DNA host. In relation to this model, the partially oxidized Ag_{10} violet cluster is distinct because it is compact and because it has a relatively high excitation energy. We suggest that these differences may reflect the flexibility of silver clusters and are now extending our studies to the fluorescent counterparts of the precursor violet clusters.[37,102]

Encapsulating DNA−Ag^+ Shell. The oligonucleotide frames the overall DNA−cluster complex. Size exclusion chromatography shows that the oligonucleotide wraps around the cluster because the complex has a 20% smaller hydrodynamic radius than the native oligonucleotide (Figure S2).[25] This interaction is mediated by the nucleobases, and the mass and EXAFS spectra support Ag^+ bonding with the heterocyclic nitrogens (Figures S11 and 4 and Table 2). We propose that this DNA−Ag^+ shell acts as a chiral footprint and induces chirality in the underlying metal-like core.[65,103−106] This interaction is multivalent and long-ranged because only DNA strands with $\gtrsim$ 20 nucleobases maintain the cluster chirality.

DOI: 10.1021/jacs.5b13124
J. Am. Chem. Soc. 2016, 138, 3469−3477

The average silver−nucleobase coordination number of 1.02 ± 0.16 silvers:nucleobase suggests that these interactions are also intermittent, so the nucleobase−Ag^+ contact points are bridged by intervening nucleobases that do not coordinate the cluster. Thus, the polymeric backbone constrains how the DNA ligand coordinates its cluster adduct.[107] This model prompts two questions: Does an immutable and rigid cluster guide the DNA coordination and wrapping or does the DNA strand mold the structure of a flexible cluster adduct? In the former case, the rigid structure of the cluster defines specific contact points for a pliable polymeric DNA.[108,109] In the latter case, the DNA sequence and structure control the three-dimensional array of nucleobases that bind and anchor a flexible cluster.[37,102] We are now studying alternate sequences that evaluate the relative importance of these cluster-based versus DNA-based factors.

Shell−Core Linkage. These studies characterize a silver cluster that is both highly oxidized yet also metal-like. The high Ag−Ag coordination number and the short Ag−Ag bond length suggest that the reduced silvers partition into a core, while the oxidized silvers segregate to the periphery. The third peak in the EXAFS spectrum suggests that these two types of silver are coupled. The associated bond length of 3.37 ± 0.02 Å is comparable to the sum of the van der Waal radii for silver of 3.44 Å.[79] Two other observations support a multivalent and dynamic association between these two components. First, the coordination number of 3.6 ± 1.7 is large and indicates that multiple Ag atoms interact at this distance. Second, the Debye−Waller factor is 2.4-times larger in relation to the Ag−Ag bonding in the core and thus supports a dynamic association between the two components.

We now consider these loose silver−silver interactions in the context of the DNA scaffold. The 20-nucleobase strand has a hydrodynamic radius of ∼1 nm, so the 10 silvers have a local concentration of ∼4 M. Such high local concentrations could promote argentophilic, Ag^+−Ag^+ bonding, as in inorganic complexes.[76,82] However, these interactions have bond strengths of 5−15 kcal/mol, so they may be disrupted by the DNA host. In support, consecutive silvers in duplex DNA show a limited tendency to self-associate.[110] Thus, we suggest that silver−silver bonds in the core and silver−DNA bonds in the shell dominate the structure, and the interaction between the two components is weak. Temperature-dependent EXAFS studies may provide further insight into this association and thus guide our continuing efforts to modulate the cluster environments and spectra.[19,111]

CONCLUSION

We described a specific violet cluster−DNA complex that organizes into two distinct structural components. The metal-like core has highly coordinated and short silver−silver bonds, and these characteristics support the subvalent cluster Ag_6^{2+} with an octahedral geometry. Such a structure is distinct from the fully reduced cores observed with thiolated silver clusters and suggests that silver clusters can adopt a range of structures and charge states.[112] The ligand shell is a 20-nucleobase DNA strand, and our studies suggest that it preferentially coordinates the remaining 4 Ag^+ that are not in the core. These two components are coupled by long-range and dynamic silver−silver interactions. Theoretical studies may provide further insight into this suggested structure. These studies provide the foundation to evaluate corresponding fluorescent analogs and to ultimately address the underlying basis for fluorescence switching by this cluster.

ASSOCIATED CONTENT

Supporting Information

The Supporting Information is available free of charge on the ACS Publications website at DOI: 10.1021/jacs.5b13124.

Figures describing size exclusion chromatograms of the native and cluster-bearing DNA strands, mass and mass:charge spectra of a longer oligonucleotide with the violet cluster, absorption spectra of violet clusters with the DNA templates from Table 1, mass:charge spectra of the native 20-nucleotide DNA in its −6 charge state, isotope model for the −6 charge state, mass:charge spectra of the −4 to −12 charge states for the violet cluster/DNA complexes, mass:charge spectrum of the 20-nucleotide DNA with the violet cluster in ammonium acetate, mass:charge spectra of the −4 to −11 charge states for the violet cluster/DNA complexes in a ammonium acetate buffer, mass:charge spectra of the −5, −7, −8, −9, −10, and −11 charge states for the Na^+ complexes, mass spectra of Ag^+-DNA complexes, circular dichroism spectra of the violet cluster with the 20 nucleotide strand at different temperatures, and the EXAFS oscillations are shown in k-space (PDF)

AUTHOR INFORMATION

Corresponding Author

*jeff.petty@furman.edu

Author Contributions

§These authors contributed equally.

Notes

The authors declare no competing financial interest.

ACKNOWLEDGMENTS

We thank the National Institutes of Health (1R15GM102818) and the Beckman Foundation. J.T.P. is supported through the Henry Keith and Ellen Hard Townes Professorship. O.O.S. is supported by a fellowship from the Furman Advantage Program. D.M.C. is supported by the NSERC CGS-Alexander Graham Bell scholarship. P.Z. acknowledges the NSERC Discovery Grant for funding. CLS@APS facilities (Sector 20) at the Advanced Photon Source (APS) are supported by the U.S. Department of Energy (DOE), NSERC Canada, the University of Washington, the Canadian Light Source (CLS), and the APS. Use of the APS is supported by the DOE under Contract No. DE-AC02−06CH11357. The CLS is financially supported by NSERC Canada, CIHR, NRC, and the University of Saskatchewan. Technical support at SXRMB (CLS) facilities from Aimee MacLennan, Dr. Qunfeng Xiao, and Dr. Yongfeng Hu is acknowledged. Technical support at CLS@APS (Sector 20, APS) facilities from Dr. Robert Gordon and Dr. Zou Finfrock is acknowledged. We greatly appreciate conversations with R. Dickson.

REFERENCES

(1) Bakr, O. M.; Amendola, V.; Aikens, C. M.; Wenseleers, W.; Li, R.; Dal Negro, L.; Schatz, G. C.; Stellacci, F. *Angew. Chem., Int. Ed.* **2009**, *48*, 5921−5926.

(2) Lecoultre, S.; Rydlo, A.; Buttet, J.; Félix, C.; Gilb, S.; Harbich, W. *J. Chem. Phys.* **2011**, *134*, 184504.

(3) Joshi, C. P.; Bootharaju, M. S.; Bakr, O. M. *J. Phys. Chem. Lett.* **2015**, *6*, 3023−3035.

(4) Joshi, C. P.; Bootharaju, M. S.; Alhilaly, M. J.; Bakr, O. M. *J. Am. Chem. Soc.* **2015**, *137*, 11578−11581.

DOI: 10.1021/jacs.5b13124
J. Am. Chem. Soc. 2016, 138, 3469−3477

(5) Conn, B. E.; Desireddy, A.; Atnagulov, A.; Wickramasinghe, S.; Bhattarai, B.; Yoon, B.; Barnett, R. N.; Abdollahian, Y.; Kim, Y. W.; Griffith, W. P.; Oliver, S. R. J.; Landman, U.; Bigioni, T. P. *J. Phys. Chem. C* **2015**, *119*, 11238−11249.
(6) Zheng, K.; Yuan, X.; Goswami, N.; Zhang, Q.; Xie, J. *RSC Adv.* **2014**, *4*, 60581−60596.
(7) Obliosca, J. M.; Babin, M. C.; Liu, C.; Liu, Y. L.; Chen, Y. A.; Batson, R. A.; Ganguly, M.; Petty, J. T.; Yeh, H. C. *ACS Nano* **2014**, *8*, 10150−10160.
(8) Ashenfelter, B. A.; Desireddy, A.; Yau, S. H.; Goodson, T.; Bigioni, T. P. *J. Phys. Chem. C* **2015**, *119*, 20728−20734.
(9) Lavis, L. D.; Raines, R. T. *ACS Chem. Biol.* **2008**, *3*, 142−155.
(10) Lavis, L. D.; Raines, R. T. *ACS Chem. Biol.* **2014**, *9*, 855−866.
(11) Resch-Genger, U.; Grabolle, M.; Cavaliere-Jaricot, S.; Nitschke, R.; Nann, T. *Nat. Methods* **2008**, *5*, 763−775.
(12) Wegner, K. D.; Hildebrandt, N. *Chem. Soc. Rev.* **2015**, *44*, 4792−4834.
(13) Enterina, J. R.; Wu, L.; Campbell, R. E. *Curr. Opin. Chem. Biol.* **2015**, *27*, 10−17.
(14) Zheng, J.; Zhou, C.; Yu, M.; Liu, J. *Nanoscale* **2012**, *4*, 4073−4083.
(15) Bousquet, B.; Cherif, M.; Huang, K.; Rabilloud, F. *J. Phys. Chem. C* **2015**, *119*, 4268−4277.
(16) Petty, J. T.; Zheng, J.; Hud, N. V.; Dickson, R. M. *J. Am. Chem. Soc.* **2004**, *126*, 5207−5212.
(17) Gwinn, E.; Schultz, D.; Copp, S.; Swasey, S. *Nanomaterials* **2015**, *5*, 180−207.
(18) Liu, J. *TrAC, Trends Anal. Chem.* **2014**, *58*, 99−111.
(19) Petty, J. T.; Story, S. P.; Hsiang, J. C.; Dickson, R. M. *J. Phys. Chem. Lett.* **2013**, *4*, 1148−1155.
(20) Obliosca, J. M.; Liu, C.; Batson, R. A.; Babin, M. C.; Werner, J. H.; Yeh, H.-C. *Biosensors* **2013**, *3*, 185−200.
(21) Latorre, A.; Somoza, Á. *ChemBioChem* **2012**, *13*, 951−958.
(22) Han, B. Y.; Wang, E. K. *Anal. Bioanal. Chem.* **2012**, *402*, 129−138.
(23) Daune, M.; Dekker, C. A.; Schachman, H. K. *Biopolymers* **1966**, *4*, 51−76.
(24) Jensen, R. H.; Davidson, N. *Biopolymers* **1966**, *4*, 17−32.
(25) Petty, J. T.; Sergev, O. O.; Kantor, A. G.; Rankine, I. J.; Ganguly, M.; David, F. D.; Wheeler, S. K.; Wheeler, J. F. *Anal. Chem.* **2015**, *87*, 5302−5309.
(26) Brust, M.; Walker, M.; Bethell, D.; Schiffrin, D. J.; Whyman, R. *J. Chem. Soc., Chem. Commun.* **1994**, *0*, 801−802.
(27) Vosch, T.; Antoku, Y.; Hsiang, J.-C.; Richards, C. I.; Gonzalez, J. I.; Dickson, R. M. *Proc. Natl. Acad. Sci. U. S. A.* **2007**, *104*, 12616−12621.
(28) Richards, C. I.; Choi, S.; Hsiang, J.-C.; Antoku, Y.; Vosch, T.; Bongiorno, A.; Tzeng, Y.-L.; Dickson, R. M. *J. Am. Chem. Soc.* **2008**, *130*, 5038−5039.
(29) Sharma, J.; Yeh, H. C.; Yoo, H.; Werner, J. H.; Martinez, J. S. *Chem. Commun.* **2010**, *46*, 3280−3282.
(30) Schultz, D.; Gardner, K.; Oemrawsingh, S. S. R.; Markešević, N.; Olsson, K.; Debord, M.; Bouwmeester, D.; Gwinn, E. *Adv. Mater.* **2013**, *25*, 2797−2803.
(31) Copp, S. M.; Bogdanov, P.; Debord, M.; Singh, A.; Gwinn, E. *Adv. Mater.* **2014**, *26*, 5839−5845.
(32) Yeh, H. C.; Sharma, J.; Han, J. J.; Martinez, J. S.; Werner, J. H. *Nano Lett.* **2010**, *10*, 3106−3110.
(33) Petty, J. T.; Sengupta, B.; Story, S. P.; Degtyareva, N. N. *Anal. Chem.* **2011**, *83*, 5957−5964.
(34) Petty, J. T.; Giri, B.; Miller, I. C.; Nicholson, D. A.; Sergev, O. O.; Banks, T. M.; Story, S. P. *Anal. Chem.* **2013**, *85*, 2183−2190.
(35) Petty, J. T.; Sergev, O. O.; Nicholson, D. A.; Goodwin, P. M.; Giri, B.; McMullan, D. R. *Anal. Chem.* **2013**, *85*, 9868−9876.
(36) Chevrier, D. M.; Yang, R.; Chatt, A.; Zhang, P. *Nanotechnol. Rev.* **2015**, *4*, 193.
(37) Bonacic-Koutecky, V.; Veyret, V.; Mitric, R. *J. Chem. Phys.* **2001**, *115*, 10450−10460.
(38) Gell, L.; Kulesza, A.; Petersen, J.; Röhr, M. I. S.; Mitrić, R.; Bonačić-Koutecký, V. *J. Phys. Chem. C* **2013**, *117*, 14824−14831.
(39) Aikens, C. M. *J. Phys. Chem. Lett.* **2011**, *2*, 99−104.
(40) Padmos, J. D.; Zhang, P. *J. Phys. Chem. C* **2012**, *116*, 23094−23101.
(41) MacDonald, M. A.; Chevrier, D. M.; Zhang, P.; Qian, H.; Jin, R. *J. Phys. Chem. C* **2011**, *115*, 15282−15287.
(42) Mann, M.; Meng, C. K.; Fenn, J. B. *Anal. Chem.* **1989**, *61*, 1702−1708.
(43) Griffeycor, R. H.; Sasmor, H.; Greig, M. J. *J. Am. Soc. Mass Spectrom.* **1997**, *8*, 155−160.
(44) Huber, C. G.; Oberacher, H. *Mass Spectrom. Rev.* **2001**, *20*, 310−343.
(45) Zhang, P.; Sham, T. K. *Phys. Rev. Lett.* **2003**, *90*, 245502.
(46) Ankudinov, A. L.; Ravel, B.; Rehr, J. J.; Conradson, S. D. *Phys. Rev. B: Condens. Matter Mater. Phys.* **1998**, *58*, 7565−7576.
(47) Newville, M.; Boyanov, B. I.; Sayers, D. E. *J. Synchrotron Radiat.* **1999**, *6*, 264−265.
(48) Newville, M. *J. Synchrotron Radiat.* **2001**, *8*, 322−324.
(49) Ravel, B.; Newville, M. *J. Synchrotron Radiat.* **2005**, *12*, 537−541.
(50) Padmos, J. D.; Personick, M. L.; Tang, Q.; Duchesne, P. N.; Jiang, D.-E.; Mirkin, C. A.; Zhang, P. *Nat. Commun.* **2015**, *6*, 7664.
(51) Leroy, J. L.; Gehring, K.; Kettani, A.; Gueron, M. *Biochemistry* **1993**, *32*, 6019−6031.
(52) Yamane, T.; Davidson, N. *Biochim. Biophys. Acta* **1962**, *55*, 609−621.
(53) Guo, J.; Kumar, S.; Bolan, M.; Desireddy, A.; Bigioni, T. P.; Griffith, W. P. *Anal. Chem.* **2012**, *84*, 5304−5308.
(54) Ritchie, C. M.; Johnsen, K. R.; Kiser, J. R.; Antoku, Y.; Dickson, R. M.; Petty, J. T. *J. Phys. Chem. C* **2007**, *111*, 175−181.
(55) Sengupta, B.; Ritchie, C. M.; Buckman, J. G.; Johnsen, K. R.; Goodwin, P. M.; Petty, J. T. *J. Phys. Chem. C* **2008**, *112*, 18776−18782.
(56) Koszinowski, K.; Ballweg, K. *Chem. - Eur. J.* **2010**, *16*, 3285−3290.
(57) Copp, S. M.; Schultz, D.; Swasey, S.; Pavlovich, J.; Debord, M.; Chiu, A.; Olsson, K.; Gwinn, E. *J. Phys. Chem. Lett.* **2014**, *5*, 959−963.
(58) Yergey, J.; Heller, D.; Hansen, G.; Cotter, R. J.; Fenselau, C. *Anal. Chem.* **1983**, *55*, 353−356.
(59) Kilgour, D. P. A.; Van Orden, S. L.; Tran, B. Q.; Goo, Y. A.; Goodlett, D. R. *Anal. Chem.* **2015**, *87*, 5797−5801.
(60) Brownawell, M. L.; San Filippo, J. *J. Chem. Educ.* **1982**, *59*, 663.
(61) Comeau, A. N.; Liu, J.; Khadka, C. B.; Corrigan, J. F.; Konermann, L. *Anal. Chem.* **2013**, *85*, 1200−1207.
(62) Greig, M. J.; Gaus, H.-J.; Griffey, R. H. *Rapid Commun. Mass Spectrom.* **1996**, *10*, 47−50.
(63) Manning, G. S. *Q. Rev. Biophys.* **1978**, *11*, 179−246.
(64) Shui, X.; McFail-Isom, L.; Hu, G. G.; Williams, L. D. *Biochemistry* **1998**, *37*, 8341−8355.
(65) Swasey, S. M.; Karimova, N.; Aikens, C. M.; Schultz, D. E.; Simon, A. J.; Gwinn, E. G. *ACS Nano* **2014**, *8*, 6883−6892.
(66) Dolamic, I.; Knoppe, S.; Dass, A.; Bürgi, T. *Nat. Commun.* **2012**, *3*, 798.
(67) Soto-Verdugo, V.; Metiu, H.; Gwinn, E. *J. Chem. Phys.* **2010**, *132*, 195102.
(68) Knoppe, S.; Bürgi, T. *Acc. Chem. Res.* **2014**, *47*, 1318−1326.
(69) Nilsson, K. B.; Persson, I.; Kessler, V. G. *Inorg. Chem.* **2006**, *45*, 6912−6921.
(70) Kistenmacher, T. J.; Rossi, M.; Marzilli, L. G. *Inorg. Chem.* **1979**, *18*, 240−244.
(71) Menzer, S.; Sabat, M.; Lippert, B. *J. Am. Chem. Soc.* **1992**, *114*, 4644−4649.
(72) Yamaguchi, T.; Wakita, H.; Nomura, M. *J. Chem. Soc., Chem. Commun.* **1988**, 433−434.
(73) Cardini, G.; Muniz-Miranda, M.; Schettino, V. *J. Phys. Chem. B* **2004**, *108*, 17007−17011.
(74) Eichhorn, G. L.; Butzow, J. J.; Clark, P.; Tarien, E. *Biopolymers* **1967**, *5*, 283−296.
(75) Shin, Y. A.; Eichhorn, G. L. *Biopolymers* **1980**, *19*, 539−556.

DOI: 10.1021/jacs.5b13124
J. Am. Chem. Soc. 2016, 138, 3469−3477

(76) Schmidbaur, H.; Schier, A. *Angew. Chem., Int. Ed.* **2015**, *54*, 746−784.
(77) Desireddy, A.; Conn, B. E.; Guo, J.; Yoon, B.; Barnett, R. N.; Monahan, B. M.; Kirschbaum, K.; Griffith, W. P.; Whetten, R. L.; Landman, U.; Bigioni, T. P. *Nature* **2013**, *501*, 399−402.
(78) Yang, H.; Wang, Y.; Huang, H.; Gell, L.; Lehtovaara, L.; Malola, S.; Häkkinen, H.; Zheng, N. *Nat. Commun.* **2013**, *4*, 2422.
(79) Bondi, A. *J. Phys. Chem.* **1964**, *68*, 441−451.
(80) Belanger-Gariepy, F.; Beauchamp, A. L. *J. Am. Chem. Soc.* **1980**, *102*, 3461−3464.
(81) Petty, J. T.; Nicholson, D. A.; Sergev, O. O.; Graham, S. K. *Anal. Chem.* **2014**, *86*, 9220−9228.
(82) Jansen, M. *Angew. Chem., Int. Ed. Engl.* **1987**, *26*, 1098−1110.
(83) Lewis, G. N. *J. Am. Chem. Soc.* **1916**, *38*, 762−785.
(84) Kossel, W. *Ann. Phys.* **1916**, *354*, 229−362.
(85) Linke, C.; Jansen, M. *Inorg. Chem.* **1994**, *33*, 2614−2616.
(86) Behrens, P.; Assmann, S.; Bilow, U.; Linke, C.; Jansen, M. *Z. Anorg. Allg. Chem.* **1999**, *625*, 111−116.
(87) Kikukawa, Y.; Kuroda, Y.; Suzuki, K.; Hibino, M.; Yamaguchi, K.; Mizuno, N. *Chem. Commun.* **2013**, *49*, 376−378.
(88) Kim, Y.; Seff, K. *J. Am. Chem. Soc.* **1977**, *99*, 7055−7057.
(89) Kulesza, A.; Mitrić, R.; Bonačić-Koutecký, V.; Bellina, B.; Compagnon, I.; Broyer, M.; Antoine, R.; Dugourd, P. *Angew. Chem., Int. Ed.* **2011**, *50*, 878−881.
(90) Yang, H.; Lei, J.; Wu, B.; Wang, Y.; Zhou, M.; Xia, A.; Zheng, L.; Zheng, N. *Chem. Commun.* **2013**, *49*, 300−302.
(91) Argay, G.; Naraysza, I. *Acta Chim. Acad. Sci. Hung.* **1966**, *49*, 329.
(92) Schreyer, M.; Jansen, M. *Angew. Chem., Int. Ed.* **2002**, *41*, 643−646.
(93) Nuss, J.; Dietrich, V.; Curda, J.; Jansen, M. *Z. Anorg. Allg. Chem.* **2014**, *640*, 1063−1068.
(94) Johannes, M. D.; Streltsov, S.; Mazin, I. I.; Khomskii, D. I. *Phys. Rev. B: Condens. Matter Mater. Phys.* **2007**, *75*, 180404.
(95) Chevrier, D. M.; Zeng, C. J.; Jin, R. C.; Chatt, A.; Zhang, P. *J. Phys. Chem. C* **2015**, *119*, 1217−1223.
(96) Knoppe, S.; Malola, S.; Lehtovaara, L.; Bürgi, T.; Häkkinen, H. *J. Phys. Chem. A* **2013**, *117*, 10526−10533.
(97) de Heer, W. A. *Rev. Mod. Phys.* **1993**, *65*, 611−676.
(98) Zheng, J.; Nicovich, P. R.; Dickson, R. M. *Annu. Rev. Phys. Chem.* **2007**, *58*, 409.
(99) Walter, M.; Akola, J.; Lopez-Acevedo, O.; Jadzinsky, P. D.; Calero, G.; Ackerson, C. J.; Whetten, R. L.; Gronbeck, H.; Häkkinen, H. *Proc. Natl. Acad. Sci. U. S. A.* **2008**, *105*, 9157−9162.
(100) Guidez, E. B.; Aikens, C. M. *Nanoscale* **2012**, *4*, 4190−4198.
(101) Johnson, H. E.; Aikens, C. M. *J. Phys. Chem. A* **2009**, *113*, 4445−4450.
(102) Baletto, F.; Ferrando, R. *Rev. Mod. Phys.* **2005**, *77*, 371−423.
(103) Gautier, C.; Bürgi, T. *ChemPhysChem* **2009**, *10*, 483−492.
(104) Sánchez-Castillo, A.; Noguez, C.; Garzón, I. L. *J. Am. Chem. Soc.* **2010**, *132*, 1504−1505.
(105) Yao, H.; Fukui, T.; Kimura, K. *J. Phys. Chem. C* **2007**, *111*, 14968−14976.
(106) Provorse, M. R.; Aikens, C. M. *J. Am. Chem. Soc.* **2010**, *132*, 1302−1310.
(107) Varani, G. *Annu. Rev. Biophys. Biomol. Struct.* **1995**, *24*, 379−404.
(108) Mirkin, C. A.; Letsinger, R. L.; Mucic, R. C.; Storhoff, J. J. *Nature* **1996**, *382*, 607−609.
(109) Alivisatos, A. P.; Johnsson, K. P.; Peng, X.; Wilson, T. E.; Loweth, C. J.; Bruchez, M. P.; Schultz, P. G. *Nature* **1996**, *382*, 609−611.
(110) Johannsen, S.; Megger, N.; Böhme, D.; Sigel, R. K. O.; Müller, J. *Nat. Chem.* **2010**, *2*, 229−234.
(111) Zhang, P. *J. Phys. Chem. C* **2014**, *118*, 25291−25299.
(112) Henglein, A.; Mulvaney, P.; Linnert, T. *Faraday Discuss.* **1991**, *92*, 31−44.

DOI: 10.1021/jacs.5b13124
J. Am. Chem. Soc. 2016, 138, 3469−3477